



This is the accepted manuscript made available via CHORUS. The article has been published as:

## Giant magnetoresistance in the crystalline $\text{m}_{\text{YCd}}\text{m}_{\text{6}}\text{m}_{\text{6}}$ intermetallic compound

M. Cabrera-Baez, K. V. R. A. Silva, P. R. T. Ribeiro, D. R. Ratkovski, E. L. T. França, A. Flessa-Savvidou, B. Casas, T. Siegrist, L. Balicas, S. M. Rezende, and F. L. A. Machado  
Phys. Rev. B **107**, 144414 — Published 10 April 2023

DOI: [10.1103/PhysRevB.107.144414](https://doi.org/10.1103/PhysRevB.107.144414)

# Giant magnetoresistance in crystalline $YCd_6$ intermetallic compound

M. Cabrera-Baez,<sup>1</sup> K. V. R. A. Silva,<sup>1</sup> P. R. T. Ribeiro,<sup>1</sup> D. R. Ratkovski,<sup>1</sup> E. L. T. França,<sup>1</sup> A. F. Savvidou,<sup>2,3</sup> B. Casas,<sup>2</sup> T. Siegrist,<sup>2</sup> L. Balicas,<sup>2,3</sup> S. M. Rezende,<sup>1</sup> and F. L. A. Machado<sup>1,2</sup>

<sup>1</sup>*Departamento de Física, Universidade Federal de Pernambuco, 50670-901, Recife, PE, Brazil*

<sup>2</sup>*National High Magnetic Field Laboratory, Tallahassee, FL 32310, USA*

<sup>3</sup>*Department of Physics, Florida State University, Tallahassee, FL 32306, USA*

(Dated: March 28, 2023)

Giant magnetoresistance (GMR) in bulk nonmagnetic compounds has received considerable attention since this phenomenon challenged the classical understanding of electron transport under a magnetic field. Here, we report magneto-transport properties of the diamagnetic intermetallic compound  $YCd_6$  for applied magnetic fields up to 35 T and temperatures down to 0.4 K that reveal GMR. We argue that the large MR value can be explained in terms of field induced pseudogaps on Fermi surface. These results are relevant to the understanding of the Fermi surface topology of quasicrystals approximants.

PACS numbers:

## I. INTRODUCTION

Since the discovery of giant magnetoresistance (GMR) in multilayers of Fe/Cr, magnetoresistance (MR) has become one of the most studied properties of materials due to its implications in sensor devices, magnetic memory and read head technology. Although GMR was observed in artificial multilayers [1], naturally layered compounds are an important alternative for understanding of fundamental issues concerning transport in 2D and 3D materials [2]. GMR has been observed in naturally layered magnetic and non-magnetic systems. In the first case, investigations in rare earth based intermetallic systems have been attracting attention of researchers for several decades [3,4] since the resistivity can become complex in view of the coexistence between localized and itinerant spins. The resistivity can have two major contributions from the conduction electron relaxation time and density. Recently, topological semimetals renewed the interest in this class of systems because they host intriguing magnetic and electric properties [5]. Large magnetoresistance in single crystal semimetals like  $(W,Mo)Te_2$ ,  $(Nb,Ta)Sb_2$ ,  $Cd_3As_2$ , etc has been revealed ranging from  $10^5$  % to  $10^6$  % at magnetic field around 9 T and  $T \sim 2$  K [5–8]. Besides, MR was also detected in nonmagnetic metallic systems as  $PdCoO_2$  [9] and  $PtSn_4$  [10] with high carrier density reaching  $10^4$  % to  $10^5$  % at 14 T and 2 K.

The physical explanation of MR in semimetals relies on models involving two bands resulting in large parabolic field dependent MR [11]. In the case of metals as  $PtSn_4$ , these large magnetic field effects on transport properties are mainly due to different mobility changes for the different types of carriers. The anisotropic field response on MR in  $PtSn_4$  indicates a complicated electronic structure [10]. In the same line of non-magnetic metallic systems, the case of the cubic intermetallic system  $YCd_6$  is relevant due to the connection with the icosahedral quasicrystal  $i$ -Y-Cd [12,13].  $RCd_6$  ( $R$ : rare earth) compounds are known as quasicrystal approximants (QCA) to the icosahedral quasicrystals (QC)  $i$ - $R$ -Cd [14] where

some of the QC have a long-range orientational order but lack a periodic translational order.

Up to now, no MR studies have been reported in members of the family of  $RCd_6$  because it is uncommon in non-layered systems. Particularly, the QCA  $YCd_6$  has a body-centered cubic (bcc) crystal structure (space group  $Im\bar{3}$ ) composed of the so-called Tsai-type icosahedral cluster, as shown in Fig. 1.  $YCd_6$  is an intermetallic crystalline compound with a complex unit cell characterized by a strong diamagnetic behavior almost independent of the temperature from dc magnetic susceptibility measurements [14]. This metallic system exhibits a small Sommerfeld coefficient of  $9(4)$  mJ/mol.K<sup>2</sup> giving  $1.3$  mJ/mol.K<sup>2</sup> per atom compatible with elemental metals as Cu, Al, etc [14]. These results point out  $YCd_6$  as an uncorrelated simple system.

Recently, in a microscopic point of view, ESR experiments on  $Gd^{3+}$  doped single crystals of  $YCd_6$  reveal the existence of various electronic bands at the Fermi level where a different degree of electronic localization was measured [15]. More itinerant electrons called  $s$ -type were responsible for the observed exchange bottleneck phenomena and the relaxation of the magnetic probe was also with  $p$ -type and  $d$ -type conduction electrons. The combination of the already reported DFT calculations on  $YCd_6$  [16] and the experimental study using ESR, supports unequivocally, a multiband scenario of this compound and future explorations on transport properties may take this as a starting point. Here we report GMR at low temperatures and high applied magnetic fields in  $YCd_6$  showing striking dependencies with the applied magnetic field.

## II. EXPERIMENTS

### A. Sample preparation and characterization

A batch of  $YCd_6$  single crystals was grown by the standard self-flux method [17] using an excess of Cd follow-

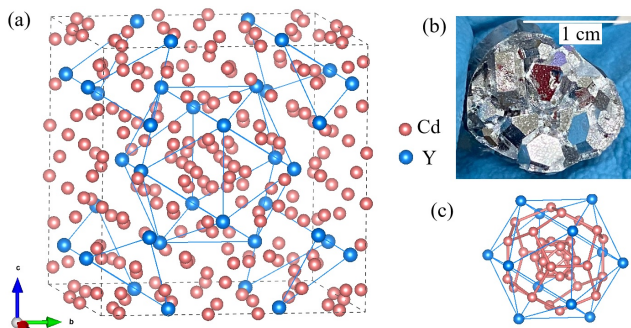


FIG. 1: (a) Crystal structure of the cubic  $\text{YCd}_6$  intermetallic system. (b) Typical polyhedral samples. (c) Cages formed by Y and Cd atoms.

ing the available phase diagram [12]. The constituent elements were 99.9% Y and 99.999% Cd (Alfa-Aesar). Initial ratios of elements were 7:93 for Y:Cd based on previously reported growths [15]. The elemental mixtures were sealed in an evacuated quartz ampoule and placed in a box furnace for the subsequent increase in temperature. Crystals were grown by slowly cooling the melt between 700 °C and 500 °C over 100 h. At 500 °C the ampoules were removed from the furnace, inverted, and placed in a centrifuge to spin off the Cd excess flux. The separated crystals are typically polyhedral of  $\sim 4$  mm or larger ( Fig. 1(b)).

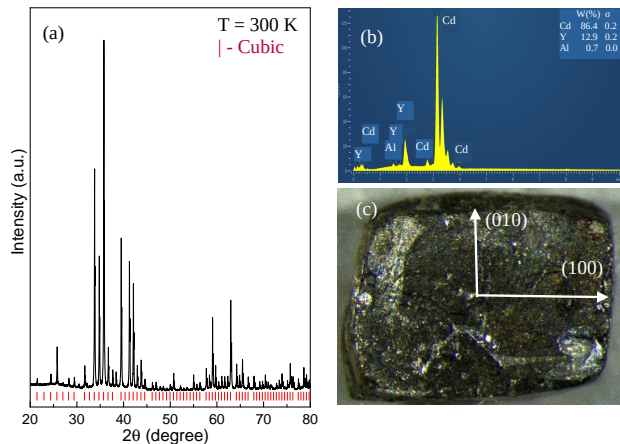


FIG. 2: (a) Room temperature X-ray diffraction data for a polycrystalline sample of  $\text{YCd}_6$ . (b) EDS spectrum and (c) a photograph indicating the (010) and (100) directions of the measured single crystal.

X-ray diffraction (XRD) of polycrystalline  $\text{YCd}_6$  was performed by using a Rigaku Smartlab diffractometer. Crystalline pieces of  $\text{YCd}_6$  were transformed into a powder sample using an agate mortar. Figure 2 shows an X-ray diffractogram obtained at room temperature collected in the angular range  $20^\circ \leq 2\theta \leq 85^\circ$  measured in steps of  $0.01^\circ$  and with an acquisition time of one second per step. The XRD data indicate that the obtained samples are single-phase and display the previously reported

crystalline structure [18]. The position of the peaks corresponds to the ones expected for a cubic phase according the ICSD-191849 [19]. Energy dispersive spectroscopy (EDS) was also used to characterize the sample yielding the composition in % of weight (wt%) with values that is very close to the nominal composition:  $\text{Y}_{12.9}\text{Cd}_{86.4}$ . A rather small peak of about 0.7 wt% of Al from the sample holder was also observed. The EDS spectrum is shown in the upper inset in Figure 2. The mass density ( $\rho_m$ ) was measured in a gas pycnometer model Accupyc II 1340 made by Micromeritics at  $T = 298$  K. A sample with mass of  $1228.6 \pm 0.1$  mg was placed in a  $10 \text{ cm}^3$  crucible filled with a helium gas atmosphere at a pressure  $1.34 \times 10^{-5}$  Pa yielding  $\rho_m = 7.65 \pm 0.13 \text{ g/cm}^3$ .

MR measurements for the temperature range  $2 \text{ K} \leq T \leq 300 \text{ K}$  and  $\mu_0 H$  under magnetic fields up to  $\mu_0 H = 8.5 \text{ T}$  were performed using the resistivity option of a Quantum Design Physical Properties Measurement System (PPMS). The four lead between the sample and the PPMS puck were attached with silver paint. The dc electrical current used in these measurements was 5 mA. The PPMS AC measurements modulus was employed for measuring the  $T$ -dependence of the ac magnetic susceptibility ( $\chi_{ac}$ ) in the same range of  $T$ s by keeping the magnitude of the ac magnetic field constant ( $h_{ac} = 10 \text{ Oe}$ ) and by varying the frequency ( $f$ ) from  $f = 30 \text{ Hz}$  to  $10^4 \text{ Hz}$ .

The MR was also measured at temperatures as low as  $T = 0.4 \text{ K}$  under magnetic fields up to 35 T using a four probe technique. These measurements were performed using a dc magnet equipped with a liquid  $^3\text{He}$ -cryostat in Cell 12 at the National High Magnetic Field Laboratory at Tallahassee. A calibrated Cernox thermometer connected to a LakeShore ac resistance bridge model 370 was used for measuring the  $^3\text{He}$  bath temperature. The  $\text{YCd}_6$  sample was mounted on a rotating sample holder that allowed to vary the direction of the applied magnetic field relative to the electrical current from a parallel to a perpendicular configuration. The crystallographic orientations were determined via Laue x-scattering, as depicted in Fig. 2(c), using the well-defined faces of the single crystal cut in those same directions using a diamond wire saw. The electrical contacts were also made with silver paint. A Keithley current source model 6221 was used to inject an ac electrical current through the sample along the (100) direction. The magnitude and frequency of the ac electrical current used to measure the MR were, respectively, 1.0 mA and 13.77 Hz and the voltage across the sample was measured using a Stanford Research Systems lock-in amplifier model SR860. The electrical resistance data were recorded while the magnetic field was continuously ramped with a sweep rate of 2 T/min.

## B. Experimental Results

Figure 3(a) shows the measured metallic like  $T$ -dependence of the in-plane resistivity ( $\rho$ ) of  $\text{YCd}_6$  under perpendicular magnetic field with field strengths  $\mu_0 H = 0$  T (dark blue spheres) and 8.5 T (red circles). At room temperature, the zero-field resistivity,  $\rho(\mu_0 H = 0)$ , is  $10.8 \mu\Omega\text{cm}$  and decreases monotonically with decreasing  $T$  down to  $1.2 \mu\Omega\text{cm}$  yielding a residual resistivity ratio  $RRR = 9$ . This value is slightly higher than the previously reported value for  $\text{YCd}_6$  single crystals [14] and may be related to the purity of the elemental Y. For  $\rho(\mu_0 H = 8.5)$  T it is possible to observe a similar metallic behavior above 110 K when compared with  $\rho(\mu_0 H = 0)$ . As the temperature decreases, strong differences appear below 100 K where the resistivity decreases from 100 K to  $T_m = 20.7$  K and then increases abruptly until  $T_0 = 5.68$  K is reached, followed by saturation below  $T_0$ .  $T_m$  corresponds to the temperature at which the slope of the resistivity as function of  $T$  changes from positive to negative.  $T_0$  is the temperature where the resistivity begins to saturate at low  $T$ s.

Fig. 3(b) shows the MR as a function of  $\mu_0 H$  measured at several temperatures revealing remarkable features. First, the resistivity has a relatively weak field dependence above 50 K but depends strongly on magnetic field below this temperature. Second, there is no evidence for saturation of the MR signal in the explored range of temperatures and fields. The magnetic field dependent of the MR curves are parabolic-like at high temperatures (above 50 K) but display a clear evolution towards linear behavior below 50 K.

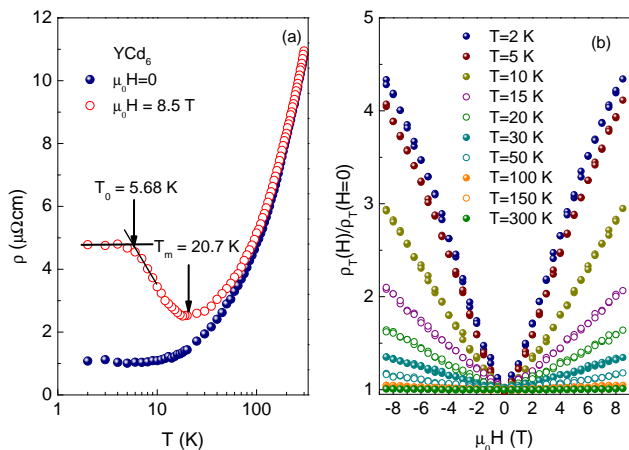


FIG. 3: (a) Resistivity vs  $T$  measured in the range 2 K - 300 K for  $\mu_0 H = 0$  and 8.5 T. Note that the resistivity becomes nearly  $T$ -independent below 5.68 K. (b) Relative resistivity versus field strength  $H$  for several values of  $T$ .

Figure 4 shows the temperature dependence of the in-phase,  $\chi'$  (a) and out-of-phase,  $\chi''$  (b) components of the ac magnetic susceptibility for  $f = 30, 50, 100, 300, 500, 1000, 3000, 5000$  and  $10000$  Hz and  $\mu_0 H_{ac} = 1$

mT applied along the (100) direction. Note that both components become nearly  $T$ -independent below some  $f$ -dependent value as indicated by  $T_{\text{cross}}$  (see Fig. 4). The insets in both figures show the linear dependence of  $T_{\text{cross}}$  yielding similar values of  $T_0 \sim 5.54$  K in (a) and  $T_0 \sim 5.87$  K in (b) at  $f = 0$  and also compatible with  $T_0 \sim 5.68$  K from Fig. 3(a). It is worth noting the clear evolution of  $\chi'$  (from  $\sim 0$  to  $-13 \times 10^{-3}$  Oe-emu/cm $^3$ ) and  $\chi''$  (from  $\sim 0$  to  $23 \times 10^{-3}$  emu/Oe-cm $^3$ ) at  $T = 2$  K for different frequencies.

As shown in Fig. 3(b), the field dependence of the MR changes between high and low temperatures. To better understand these features and complement the above information, we studied the MR under high magnetic fields.

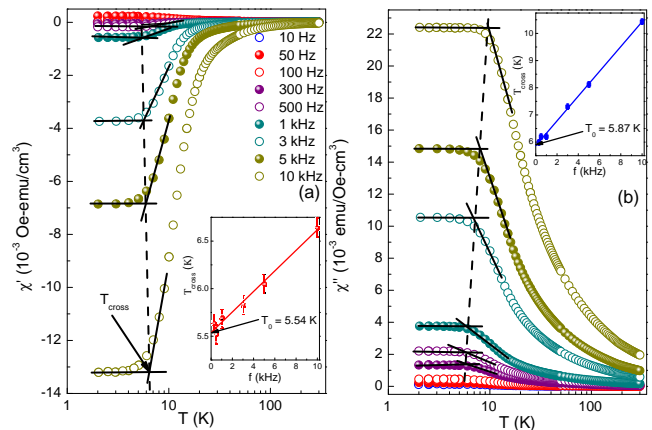


FIG. 4: Temperature dependence of the in-phase (a) and out-of-phase (b) components of the ac magnetic susceptibility for the frequencies  $f$  indicated.

Figure 5(a) presents  $\rho(\mu_0 H)$  for magnetic fields up to  $(\mu_0 H) = 35$  T (perpendicular to the electrical current) and temperatures from  $T = 25.0$  K to 0.42 K where it is possible to infer a continuous evolution on its field dependence, i.e., from linear (unsaturated) behavior ( $T \sim 25$  K) to a saturated response of  $\rho(\mu_0 H)$  at  $T \sim 0.4$  K. The data for  $T = 0.42$  K and 25 K are shown for both positive and negative values of  $H$  while for the other values of  $T$  they are shown for positive values of  $H$  only. The inset is a zoom in of the central part of the magnetoresistance data revealing that below about 50 mT the MR approaches zero in a somewhat faster magnetic field dependence, perhaps associated to a possible superconductivity transition in  $\text{YCd}_6$  and/or little residual Cd flux at the surface (EDS at various locations ensures internal homogeneity of the  $\text{YCd}_6$  sample). This low- $T$  superconducting behavior (below 1.8 K) is not relevant and does not interfere with the MR analysis. As expected, the observed linear dependence is consistent with the data presented in Fig. 3(b).

To better understand the evolution of the resistivity as a function of the magnetic field, Fig. 5(b) shows  $\rho(\mu_0 H)$  for values of  $\mu_0 H$  up to 35 T and the correspond-

ing fit to a power-law (black-line) for four values of  $T$ . The inset shows the exponent of the field dependence  $\rho(\mu_0 H) = \alpha(T)(\mu_0 H)^\eta$  featuring a linear and continuous evolution from  $\eta = 1$  to 0.5 above  $T_0 = 5.65$  K followed by saturation below  $T_0$ . A remarkable result is the  $T_0$  value that is in perfect agreement with the data presented in Fig. 3 and Fig. 4 as indicated above.

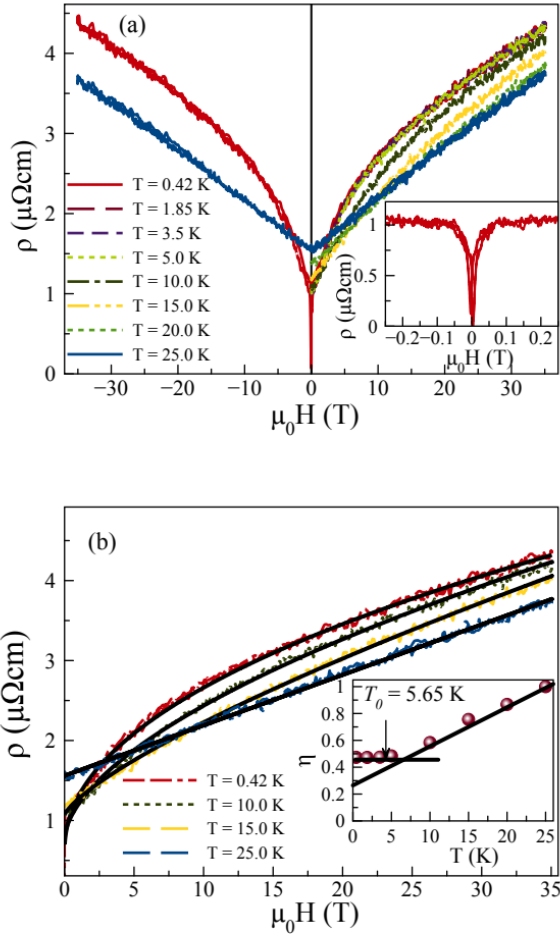


FIG. 5: (color online) (a) Low- $T$   $\rho$  versus  $H$  data for several values of  $T$  with  $H$  applied perpendicular to the electrical current. The data for  $T = 0.42$  K and 25 K are shown for both positive and negative values of  $H$  while for the other values of  $T$  are for positive values of  $H$  only. The inset is a blow-up of the central part of the magnetoresistance data. (b)  $\rho$  versus  $H$  data and the corresponding fit to a power-law (black-line) for four values of  $T$ . The inset shows the exponent of the power-law obtained for all values of  $T$ .

The single crystalline anisotropic properties of  $\rho(\mu_0 H)$  were also explored by varying the orientation of the applied magnetic field. Figure 6(a) presents  $\rho$  as a function of  $\mu_0 H$  data for several values of  $T$  with  $\mu_0 H$  applied parallel to the electrical current. The data for  $T = 0.42$  K and 25 K are shown for both positive and negative values of  $\mu_0 H$  while for the other values of  $T$  the data is dis-

played for positive values of  $\mu_0 H$  only. The inset shows the exponent of the power-law obtained for all values of  $T$  yielding values of  $\eta$  between 0.7 and 0.3. Figure 6(b) shows  $\rho$  versus  $\mu_0 H$  for several values of the angle between  $\mu_0 H$  and the electrical current. The inset shows the magnitude of the resistance for  $\mu_0 H = 35$  T obtained from a larger set of  $\rho$ - $\mu_0 H$  data. Notice that the data for  $\mu_0 H$  parallel to the electrical current is significantly smaller than the data measured with  $\mu_0 H$  perpendicular to  $I$ , as expected.

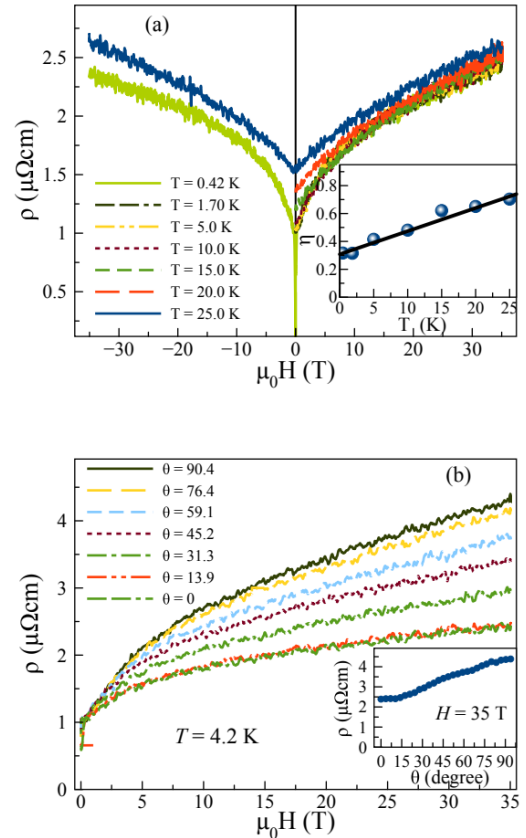


FIG. 6: (color online) (a) Low- $T$   $\rho$  versus  $\mu_0 H$  data for several values of  $T$  with  $\mu_0 H$  applied parallel to the electrical current. The inset shows the exponent of the power-law obtained for all values of  $T$ . (b) Low- $T$   $\rho$  versus  $\mu_0 H$  for several values of the angle between  $\mu_0 H$  and the electrical current. The inset shows the magnitude of the resistance for  $\mu_0 H = 35$  T obtained from a larger set of  $\rho$ - $\mu_0 H$  data.

### III. ANALYSIS AND DISCUSSION

The MR of many metals and semimetals can be represented by the form  $\Delta\rho/\rho(0) = G[H/\rho(0)]$  commonly referred to as Kohler's rule, where  $G(H)$  usually follows a power law, depending on the geometrical configurations and on the materials [20]. In a simple case of a metal, one may find the relation  $\rho/\rho(0) \sim (\omega_c \tau)^2$  where  $\omega_c = eH/m_e$

is the cyclotron frequency [21]. The observed behavior of  $\rho/\rho(0) \sim H^2$  (orbital motion of conduction electrons) is close to what is expected for an ordinary metallic compound with no open orbits [22]. For instance, this relation is satisfied by the PtSn<sub>4</sub> compound [10] (which exhibits a very large transverse magnetoresistance of  $\sim 10^5\%$ ) although its behavior differs markedly from the low  $T$  results obtained for YCd<sub>6</sub>. As shown in Figs. 3 and 5, the field dependence of the MR of YCd<sub>6</sub> evolves from  $\rho/\rho(0) \sim (\mu_0 H)^2$  above 50 K to  $\sim (\mu_0 H)^1$  ( $25 \text{ K} \leq T \leq 50 \text{ K}$ ), and to  $\sim H^{0.5}$  upon further cooling ( $0.4 \text{ K} \leq T \leq 5.65 \text{ K}$ ) in transverse MR experiments (TMR). In the case of longitudinal MR (LMR), a continuous evolution of exponent on  $\mu_0 H$ , i.e., from 0.8 to 0.3 was observed (see Fig. 6 inset).

Although the MR is not simply related to the topology of the Fermi surface (FS), the TMR and LMR data measured for YCd<sub>6</sub> at low temperatures and high magnetic fields (Fig. 3, 5, and 6) indicate anisotropy in the band structure. For YCd<sub>6</sub>, different densities of charge carriers with different mobilities that would depend on the temperature may contribute to the field dependence of  $\rho$ , leading to the super- or sublinear trends. Similar behavior was observed in PdCoO<sub>2</sub> and PtCoO<sub>2</sub> non-magnetic metallic systems [9,23]. For these systems, the  $\text{MR}(H) \sim H^{0.5}$  dependence is related to the existence of more than one length scale around the FS [23,24]. Particularly, for the case of PdCoO<sub>2</sub>, Varnavides, G, et al., proposed diffusive, ballistic, and hydrodynamic transport regime limits [25]. To compare with our data, some interesting results evidence TMR in metals at high fields as was the case of Li, Zn, Pt, Ag, Sn, Au, Ni and Pb [26] where MR of Pb followed a  $H^{0.5}$  dependence. It turns out that having two types of carriers with different mobilities can lead to sublinear MR when one is approaching its saturation. To explain the  $H^{0.5}$  and  $H^1$  behavior, the authors suggest the contact between the Brillouin-zone face and the FS. Although relevant, these experiments were carried out using polycrystals where an average over all micro-crystalline directions may contribute to the magnetic field dependence of MR. The case of YCd<sub>6</sub> shows a complete differentiation depending of the orientation of the magnetic field because we use single-crystalline samples.

For LMR results, one does not expect the motion of electrons along the field to be affected but this is only true to free electrons but not to electrons in metals [27]. Evidently, Fig. 6 shows nonzero LMR results as expected in real metals showing a saturation trend for high fields with  $T$  dependent exponents. Similar results were observed in elemental metals as Ag and Cu where the existence of necks on the FS and two types of scattering mechanisms were postulated [27]. When an electron passes through a neck, it suffers Bragg reflection and its velocity is almost exactly reversed where, at high magnetic fields, the current carried by the electrons with orbits through a neck is very reduced [27]. It is worth mentioning that the FS topology of Ag and Cu is far away to be compa-

rable with the case of YCd<sub>6</sub> for obvious reasons but, in a similar way, an LMR effect can result from FS anisotropy [20,28,29].

With this, a possible explanation of the anisotropic  $H$  dependence of MR may be related to the existence of different electron bands at the FS. Previous DFT calculations on YCd<sub>6</sub> confirm the presence of  $s$ -,  $p$ - and  $d$ -type conduction electrons and report a small midgap peak just above the Fermi level [16]. In a Fermi liquid scenario, conduction electrons with different effective masses (delocalized in energy bands) could follow different cyclotron orbits in a magnetic field. In this multiband system, it is reasonable to assume more extended orbits for  $s$ -type of conduction electrons when compared to  $p$  and  $d$  (assuming different localization degrees). Without magnetic field, the conductivity is dominated by  $s$ -,  $p$ - and  $d$ -carrier types. But with magnetic field, then it is possible that only  $s$ - type of electrons conduct. This assumption is in agreement with the observed magnetoresistive effect in Fig. 3(a). Different degree of localization of conduction electrons is a well accepted concept in view of the complex FS. Previous ESR experiments in this system support this possible scenario [15] although a detailed investigation of the Fermi surface of YCd<sub>6</sub> (experimental or theoretical) could provide better clues about a satisfactory explanation.

Other interesting system evidencing large magnetoresistance is the case of MoTe<sub>2</sub> [6] which is a noncompensated semimetal where the number of hole carriers is higher than electron carriers. This system shows nonsaturating extremely large magnetoresistance attributed to a combination of Fermi surface deformation and spin orbit interactions in the presence of external magnetic field. Similar results were observed in NbSb<sub>2</sub> [30] with strong MR anisotropy where MR is attributed to the change of the Fermi surface (Dirac-like point) induced by the magnetic field. The mechanism responsible for the observed MR is related to the creation of a gap in the two Dirac-like points induced by the external magnetic field. These observations imply the inadequacy of the FS compensation picture in NbSb<sub>2</sub> [30] in contrast with the PtSn<sub>4</sub> scenario. The case of PtSn<sub>4</sub> exhibits a minimum on the temperature dependence of the resistivity in a magnetic field due to the transition from high effective magnetic fields to weak ones [31]. This is observed in compensated conductors with a closed FS. The case of YCd<sub>6</sub> show similar results but specific electronic structure calculations exploring the FS are required to elucidate the mechanism and the effect of the magnetic field.

It is worth mentioning that Fig. 4 suggests the absence of magnetic impurities in our samples that produce a diamagnetic response. At  $T \geq 100 \text{ K}$ , the system exhibits ac frequency-independent diamagnetic character associated with a good metal. Below 100 K, YCd<sub>6</sub> presents frequency and temperature dependencies of the diamagnetic response, which is an anomalous observation [32] since frequency dependence is understood as resulting from glassiness or progressive spin freezing, and therefore

would not at all be expected for diamagnetic systems.

Although the frequency-dependent data below 100K in  $\chi'$  and  $\chi''$  reveal unusual features, one of the possible explanations of this anomalous behavior is the skin depth effect in a metal that could account for the observed anomalies. According with this idea, it is expected that  $\chi'$  becomes negligible at the maximum skin depth and the corresponding  $\chi''$  becomes maximum. In the case of the YCd<sub>6</sub>, Fig. 4a) and b) suggest that both quantities  $\chi'$  and  $\chi''$  maximize at the same frequency. With this we can rule out this hypothesis. Another point of view is to consider the existence of magnetic domains with different sizes. The emergence of diamagnetic domains (Condon domains) relates to the observation of dHvA oscillations [33] as was the case of beryllium and silver. In both cases the dHvA amplitude was comparable with the oscillation period developing Condon domains explicitly. However, as depicted in Fig. 5 and Fig. 6, there is no clear evidence of well-defined oscillations. Hence, it is possible that the dHvA amplitude (as in most metals) is significantly smaller than the oscillation period even in high quality single crystals at very low temperatures. With this, we can ignore the existence of diamagnetic domains. Since the imaginary part of the ac-susceptibility is correlated with dissipative effects in the sample, the frequency-dependent data below 100K observed in Fig. 4a) and b) suggest a strong magnetic dynamic behavior despite the lack of magnetic order. This behavior is observed in unconventional superconductors of magnetic origin [34] and in quantum magnets [35]. However, the magnetic response of a metal to an external magnetic field in a quantum-mechanical scenario of the metal's bulk properties forbids any temperature and frequency dependence of the diamagnetic behavior under ac magnetic field. These results are in agreement with the observations in ac measurements for the metal NiSi [32] where its origin is not yet understood. The ac susceptibility similarities between NiSi and YCd<sub>6</sub> are remarkable and warrant further theoretical and experimental investigations to reveal a closer perspective to the underlying mechanism.

## IV. CONCLUSIONS

Our experimental results show giant magnetoresistance in YCd<sub>6</sub> at low temperatures and high magnetic fields. MR has a field dependence evolution of  $\rho/\rho(0)$ ;  $\sim \mu_0 H^2$  above 50 K,  $\sim \mu_0 H^1$  (from 25 K to 50 K) and  $\sim \mu_0 H^{0.5}$  (from 0.4 K to 5.65 K) in transverse TMR experiments together with a continuous evolution from  $\mu_0 H^{0.8}$  to  $\mu_0 H^{0.3}$  in LMR experiments. When compared with elemental metals as Ag and Cu, LMR experiments in YCd<sub>6</sub> shows a similar saturation up to high fields suggesting a complex FS. These results indicate strong anisotropy in the band structure and a magnetic field dependence of the FS topology.

The observed magnetoresistive effect could be explained considering different  $T$  dependent mobilities for different electronic bands. The sublinear exponent can be understood as resulting as electron and hole band having different carrier densities, or lack of compensation, and different mobilities. Exploring MR in this QCA system is a fundamental task in understanding of the electronic structure, Fermi surfaces and general electronic properties of periodic systems providing the basis for the interpretation of electronic properties in more complex systems as QC's.

## Acknowledgments

The work at UFPE was supported by Brazilian agencies FACEPE, CNPq, FINEP and CAPES. The National High Magnetic Field Laboratory is supported by the National Science Foundation through NSF/DMR-1644779 and the State of Florida. L.B. is supported by the US-DOE through the BES program award DE-SC0002613

<sup>1</sup> M. N. Baibich, J. M. Broto, A. Fert, F. Nguyen Van Dau, F. Petroff, P. Etienne, G. Creuzet, A. Friederich, and J. Chazelas, Phys. Rev. Lett. **61** 2472 (1988).

<sup>2</sup> R. B. van Dover, E. M. Gyorgy, R. J. Cava, J. J. Krajewski, R. J. Felder, and W. F. Peck, Phys. Rev. B **47** 6134 (1993).

<sup>3</sup> L. Morellon, P. A. Algarabel, C. Magen, M. R. Ibarra, J. Magn. Magn. Mater. **237** 119, (2001).

<sup>4</sup> J. Sakurai, S. Nakatani, A. Adam, and H. Fujiwara, J. Magn. Magn. Mater. **108** 143, (1992).

<sup>5</sup> R. Jha, S. Onishi, R. Higashinaka, T. D. Matsuda, R. A. Ribeiro, and Y. Aoki, AIP Adv. **8** 101332, (2018).

<sup>6</sup> S. Thirupathiah, R. Jha, B. Pal, J. S. Matias, P. Kumar Das, P. K. Sivakumar, I. Vobornik, N. C. Plumb, M. Shi, R. A. Ribeiro, and D. D. Sarma, Phys. Rev. B **95** 241105(R)

(2017).

<sup>7</sup> A. Pariari, R. Singha, S. Roy, B. Satpati, and P. Mandal,, Sci. Rep. **8** 10527, (2018).

<sup>8</sup> P. Kumar, Sudesh and S. Patnaik, J. Phys. Commun. **3** 115007, (2019).

<sup>9</sup> H. Takatsu, J. J. Ishikawa, S. Yonezawa, H. Yoshino, T. Shishidou, T. Oguchi, K. Murata, and Y. Maeno, Phys. Rev. Lett. **111** 056601 (2013).

<sup>10</sup> E. Mun, H. Ko, G. J. Miller, G. D. Samolyuk, S. L. Bud'Ko, and P. C. Canfield, Phys. Rev. B **85** 035135 (2012).

<sup>11</sup> S. Zhang, Q. Wu, Y. Liu, and O. v. Yazyev, Phys. Rev. B **99** 035142 (2019).

<sup>12</sup> A. I. Goldman, T. Kong, A. Kreyssig, A. Jesche, M. Ra-

- mazanoglu, K. W. Dennis, S. L. Bud'ko and P. C. Canfield, *Nat. Mater.*, **12** 714 (2013).
- <sup>13</sup> T. Kong, S. L. Bud'ko, A. Jesche, J. McArthur, A. Kreyssig, A. I. Goldman, and P. C. Canfield, *Phys. Rev. B* **90** 014424 (2014).
- <sup>14</sup> A. Mori, H. Ota, S. Yoshiuchi, K. Iwakawa, Y. Taga, Y. Hirose, T. Takeuchi, E. Yamamoto, Y. Haga, F. Honda, et al. *J. Phys. Soc. Jpn.* **81** 024720 (2012).
- <sup>15</sup> M. Cabrera-Baez, M. A. Avila, and C. Rettori, *Phys. Rev. B* **100** 014207 (2019).
- <sup>16</sup> Y. Ishii, T. Fujiwara, *J. Alloys Compd.* **342** 343 (2002).
- <sup>17</sup> P. C. Canfield and Z. Fisk, *Phil. Mag.* **65**, 1117 (1992).
- <sup>18</sup> S. K. Dhar, A. Palenzona, P. Manfrinetti and S. M. Patilwar, *J. Phys.: Condens. Matter* **14** 517 (2002).
- <sup>19</sup> C. P. Gómez and S. Lidin, *Phys. Rev. B* **68** 024203 (2003).
- <sup>20</sup> A. B. Pippard, *Magnetoresistance in metals* (Cambridge University Press, UK, 2009).
- <sup>21</sup> J. M. D. Coey, *Magnetism and Magnetic Materials* (Cambridge, Cambridge, 2009).
- <sup>22</sup> J. M. Ziman, *Electrons and Phonons: The Theory of Transport Phenomena in Solids* (Oxford University Press, UK, 2001).
- <sup>23</sup> N. Nandi, T. Scaffidi, P. Kushwaha, S. Khim, M. E. Barber, V. Sunko, F. Mazzola, P. D. C. King, H. Rosner, P. J. W. Moll, et al. *npj Quantum Mater.* **3** 66 (2018).
- <sup>24</sup> B. N. Narozhny, *Riv. del Nuovo Cim.* **45** 661 (2022).
- <sup>25</sup> G. Varnavides, Y. Wang, P. J. W. Moll, P. Anikeeva, and P. Narang, *Phys. Rev. Mater.* **6** 045002 (2022).
- <sup>26</sup> B. Lüthi, *Phys. Rev. Lett.* **2** 503 (1959).
- <sup>27</sup> J. O. Strom-Olsen, *Proc. R. Soc. A: Math. Phys. Eng. Sci.*, **302** 1468 (1967).
- <sup>28</sup> H. K. Pal and D. L. Maslov, *Phys. Rev. B* **81** 214438 (2010).
- <sup>29</sup> A. B. Pippard, *Proc. R. Soc. A: Math. Phys. Eng. Sci.*, **282** 1391 (1964).
- <sup>30</sup> K. Wang, D. Graf, L. Li, L. Wang, and C. Petrovic, *Sci Rep* **4**, 7328 (2014).
- <sup>31</sup> A. N. Perevalova, S. V. Naumov, S. M. Podgornykh, E. B. Marchenkova, V. V. Chistyakov, J. C. A. Huang, and V. V. Marchenkov, *AIP Advances* **12**, 035225 (2022).
- <sup>32</sup> A. Dahal, J. Gunasekera, L. Harriger, S. H. Lee, Y. S. Hor, D. J. Singh, and D. K. Singh, *Phys. Rev. B* **94** 184516 (2016).
- <sup>33</sup> V. S. Egorov, *Phys.-Usp.* **53** 755 (2010).
- <sup>34</sup> S. H. Lee, H. Kikuchi, Y. Qiu, B. Lake, Q. Huang, K. Habicht, and K. Kiefer, *Nature Mater.* **6**, 853 (2007).
- <sup>35</sup> J. M. Tranquada, H. Woo, T. G. Perring, H. Goka, G. D. Gu, G. Xu, M. Fujita, and K. Yamada, *Nature* **429**, 534 (2004).